Vol 452|13 March 2008|doi:10.1038/nature06597

LETTERS

Hierarchical self-assembly of DNA into symmetric supramolecular polyhedra

Yu He[1], Tao Ye[1], Min Su[2], Chuan Zhang[1], Alexander E. Ribbe[1], Wen Jiang[2] & Chengde Mao[1]

DNA is renowned for its double helix structure and the base pairing that enables the recognition and highly selective binding of complementary DNA strands. These features, and the ability to create DNA strands with any desired sequence of bases, have led to the use of DNA rationally to design various nanostructures and even execute molecular computations[1–4]. Of the wide range of self-assembled DNA nanostructures reported, most are one- or two-dimensional[5–9]. Examples of three-dimensional DNA structures include cubes[10], truncated octahedra[11], octohedra[12] and tetrahedra[13,14], which are all comprised of many different DNA strands with unique sequences. When aiming for large structures, the need to synthesize large numbers (hundreds) of unique DNA strands poses a challenging design problem[9,15]. Here, we demonstrate a simple solution to this problem: the design of basic DNA building units in such a way that many copies of identical units assemble into larger three-dimensional structures. We test this hierarchical self-assembly concept with DNA molecules that form three-point-star motifs, or tiles. By controlling the flexibility and concentration of the tiles, the one-pot assembly yields tetrahedra, dodecahedra or buckyballs that are tens of nanometres in size and comprised of four, twenty or sixty individual tiles, respectively. We expect that our assembly strategy can be adapted to allow the fabrication of a range of relatively complex three-dimensional structures.

Our approach to forming DNA polyhedra is a one-pot self-assembly process illustrated in Fig. 1: individual single strands of DNA first assemble into sticky-ended, three-point-star motifs (tiles), which then further assemble into polyhedra through sticky-end association between the tiles. The three-point-star motif contains a threefold rotational symmetry and consists of seven strands: a long repetitive central strand (blue-red; strand L or L′), three identical medium strands (green; strand M), and three identical short peripheral strands (black; strand S). At the centre of the motif are three single-stranded loops (coloured red). The flexibility of the motif can be easily adjusted by varying the loop length, with increased loop length increasing tile flexibility. The termini of each branch of the tile carry two complementary, four-base-long, single-stranded overhangs, or sticky ends. Association between the sticky-ends allows the tiles to further assemble into larger structures such as the polyhedra described here.

The three-point-star motif has been used for the assembly of flat two-dimensional (2D) crystals[16,17], where neighbouring units face in opposite directions of the crystal plane to cancel the intrinsic curvature of the DNA tiles. Because polyhedra are closed three-dimensional (3D) objects containing a finite number of component tiles, we reasoned that three factors would promote polyhedron formation. (1) If all component DNA tiles face in the same direction, their curvatures would add up and promote the formation of closed structures. For example, some closed DNA tubular structures have been observed when all DNA tiles face the same side of the crystal plane[7]. This requirement can be easily satisfied by choosing the length of each pseudo-continuous DNA duplex in the final structures to be four turns (42 bases). (2) Self-assembly is an inter-unit process. This means that higher (micromolar) DNA concentrations favour large assemblies such as flat 2D crystals, whereas lower DNA concentrations favour small assemblies such as polyhedra. This concentration-dependent kinetic effect should also provide some control over polyhedral size. (3) 2D crystal formation was found to require loops that are two to three bases long[17]. Elongating the loops increases tile flexibility; this should prevent the assembly of DNA stars into large 2D crystals and instead promote the formation of smaller structures.

We first tested this hypothesis by assembling a DNA tetrahedron from four three-point-star tiles. Each tile sits at a vertex, and its branches each associate with a branch from another tile to form the edges of the tetrahedron. The assembled tiles at the four vertices retain the threefold rotational symmetry of the free, individual star tiles, but are no longer planar. In fact, they are significantly bent and thus need to be quite flexible. To provide this flexibility, the loop length is designed to be five bases long. This ensures that the DNA stars will associate with each other under hybridization conditions to form highly flexible assemblies, which allows the free sticky-ends in the assemblies to meet and associate with each other to yield closed

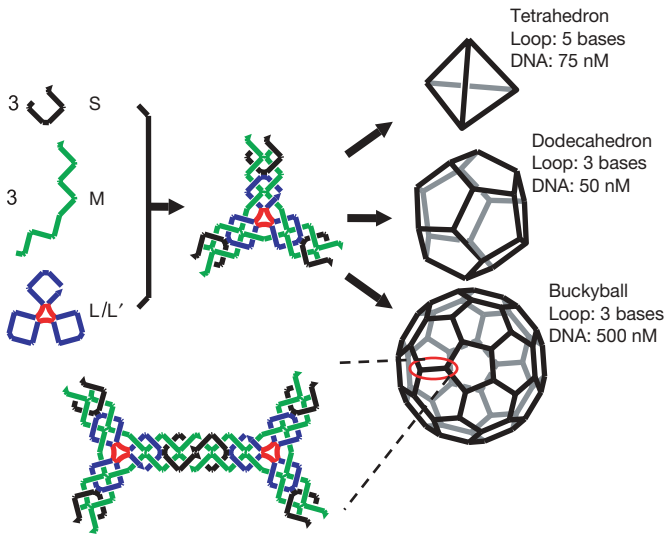

Figure 1 | Self-assembly of DNA polyhedra. Three different types of DNA single strands stepwise assemble into symmetric three-point-star motifs (tiles) and then into polyhedra in a one-pot process. There are three single-stranded loops (coloured red) in the centre of the complex. The final structures (polyhedra) are determined by the loop length (3 or 5 bases long) and the DNA concentration.

[1]Department of Chemistry, [2]Markey Center for Structural Biology and Department of Biological Sciences, Purdue University, West Lafayette, Indiana 47907, USA.

structures (without any free sticky-ends). The size of the closed structures is concentration-dependent. At sufficiently low DNA concentration, we expect the formation of tetrahedra because they are the smallest closed structures that can form without deformation of the pseudo-continuous DNA duplexes.

The DNA tetrahedra form when solutions containing the DNA strands are mixed and slowly cooled from 95 °C to room temperature (22 °C). Non-denaturing polyacrylamide gel electrophoresis (PAGE) of the resultant solution shows that for DNA concentrations of <100 nM, the dominant DNA complex contains four star tiles (Supplementary Fig. 1). Dynamic light scattering (DLS) provides a direct measurement of the physical sizes of the dissolved DNA complexes (Fig. 2a), yielding an apparent hydrodynamic radius of ~10.3 ± 0.6 nm (s.d.). This value agrees with the radius of the circumscribed sphere of the DNA tetrahedron model (10.9 nm), assuming 0.33 nm per base pair for the pitch and 2 nm for the diameter of a DNA duplex, respectively.

To provide direct evidence for the self-assembly of DNA into tetrahedra, we imaged the samples using atomic force microscopy (AFM) and cryogenic transmission electronic microscopy (cryo-EM). DNA species appear as uniform-sized, triangular particles when imaged by AFM in air (Fig. 2b). Strong electrostatic interactions with the substrate and dehydration cause the 3D DNA tetrahedron to collapse into a 2D object with a triangle shape, which is consistent with the features observed by AFM. The most convincing experimental support for tetrahedron formation comes from cryo-EM analysis (Fig. 2c, d), with the images showing that most particles have tetrahedral shapes of the expected size. The yield of correctly assembled DNA tetrahedra is ~90%, as estimated from the number of particles observed by cryo-EM and by gel electrophoretic analysis (Supplementary Fig. 2). We reconstructed from the experimentally observed particles a 3D structure for the DNA tetrahedron at 2.6 nm resolution, using single-particle 3D reconstruction[18]. The computed projections from this 3D reconstruction match well to the individual particle images (Fig. 2d) and the class averages of raw particle images with similar views (Supplementary Fig. 4). In the reconstructed 3D tetrahedron structure (Fig. 2e), the observed edges are 16 nm long, nicely matching the designed model (16.2 nm). The thickness and width of the edge is also consistent with two DNA duplexes arranged side by side in the design. At the threefold vertices, a depression is visible, which is consistent with the central cavity in star motif.

To demonstrate the versatility of the hierarchical self-assembly approach, we produced a DNA dodecahedron consisting of 20 three-point-star tiles, 12 faces (pentagons), and 30 edges. Compared to a tetrahedron, dodecahedra are less curved and the star tiles need not be nearly as flexible. Thus, the length of the central single-stranded loop is reduced to three bases long to make the star tiles much stiffer.

At a low DNA concentration (50 nM), DNA star tiles readily assemble into dodecahedra (Fig. 3). DLS measurements (Fig. 3a) reveal an apparent hydrodynamic radius for the assembled objects of ~24.0 ± 1.8 nm (s.d.), which agrees with the value (23.6 nm) estimated from the designed structural model. AFM imaging in air reveals circular features with uniform sizes (Fig. 3b) and apparent diameters of ~70 nm. This appearance of the assembled objects can be explained by DNA dehydration and strong electrostatic interactions between the DNA and mica substrate surface, which collapses the DNA dodecahedra into two layers. A close-up view (Fig. 3b inset) shows a component pentagon located at the centre of the top layer, which is in reasonable agreement with a collapsed 2D projection of a dodecahedron.

The strongest experimental evidence for dodecahedron formation is provided by cryo-EM analysis (Fig. 3c–e), which reveals dodecahedron-shaped objects of the expected size (in the boxed areas in Fig. 3c and Supplementary Fig. 6). Single-particle reconstruction using experimentally observed particles yields a 3D map of the DNA dodecahedron. An icosahedral symmetry, which shares the same symmetry as a dodecahedron, was imposed during the reconstruction, resulting in a well-defined dodecahedron structure (with a resolution of 2.8 nm). The computed projections from this 3D reconstruction match well to the individual particle images (Fig. 3d) and the class averages of raw particle images with similar views (Supplementary Fig. 7). The radius of the circumscribed sphere of the reconstructed dodecahedron model is 23.5 nm, consistent with both the design and the DLS data. Each edge is 4 nm wide and 2 nm thick,

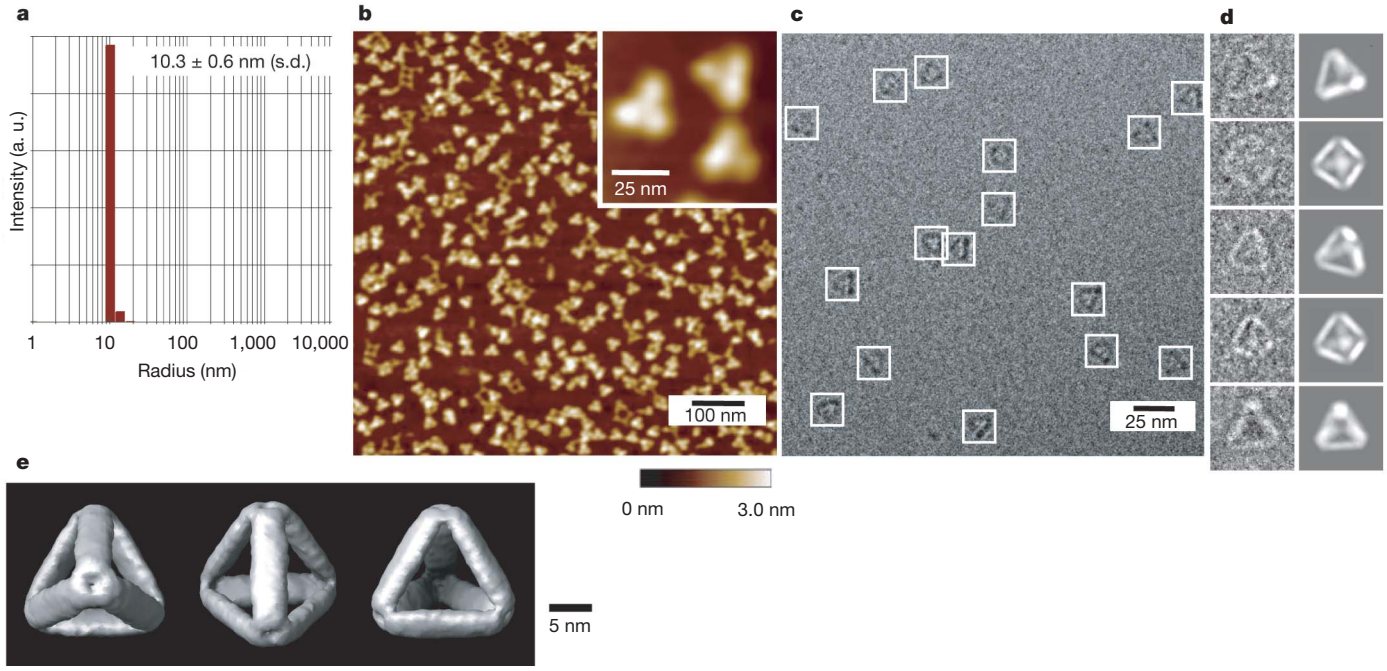

Figure 2 | Characterization of the DNA tetrahedron by DLS, AFM and Cryo-EM. a, DLS shows the size histogram of DNA tetrahedron. **b**, An AFM image of DNA tetrahedra and a close-up view (inset). A height scale bar is shown at the bottom. **c**, A representative cryo-EM image. White boxes indicate the DNA particles. For a magnified large view field, see Supplementary Fig. 3. **d**, Raw cryo-EM images of individual particles and the corresponding projections of the DNA tetrahedron 3D structure reconstructed from the cryo-EM images. These particles are selected from different image frames to represent views at different orientations. **e**, Three views of the reconstructed DNA tetrahedron structure.

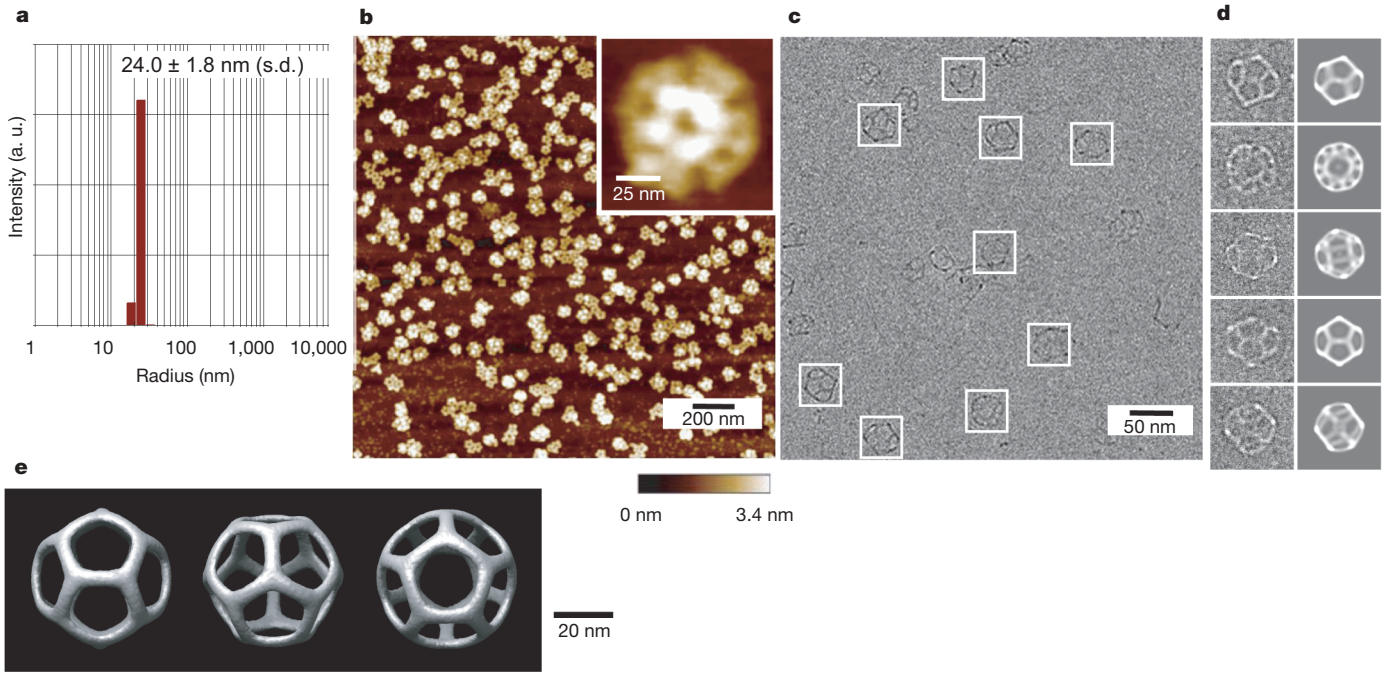

Figure 3 | A DNA dodecahedron. **a**, Size histogram of the DNA dodecahedron measured by DLS. **b**, **c**, An AFM image (**b**) and a cryo-EM image (**c**) of the DNA assemblies. For a magnified large view field, see Supplementary Fig. 6. **d**, Individual raw cryo-EM images and the corresponding projections of the DNA dodecahedron 3D structure reconstructed from cryo-EM images. These particles are selected from different image frames to represent views at different orientations. **e**, Three views of the DNA dodecahedron 3D structure.

which are reasonable dimensions for two associated branches from two neighbouring star tiles.

A truncated icosahedron structure is another type of highly symmetric polyhedron. It contains 60 vertexes, 90 edges and 32 faces (12 pentagons and 20 hexagons). Two well-known examples of such a structure are soccer balls and Buckminsterfullerene molecules (or buckyballs, C_{60}). It remains challenging to rationally design a molecular system that can self-assemble into such a complex structure. However, at a high DNA concentration (500 nM), the star tiles (with three-base-long, single-stranded loops at the centre) readily assemble into the buckyball structure—as suggested by DLS analysis, AFM imaging and cryo-EM analysis (Fig. 4). The DLS measurement indicates that the DNA assemblies have an apparent hydrodynamic radius of 42.2 ± 4.0 nm (s.d.), close to the calculated radius of the

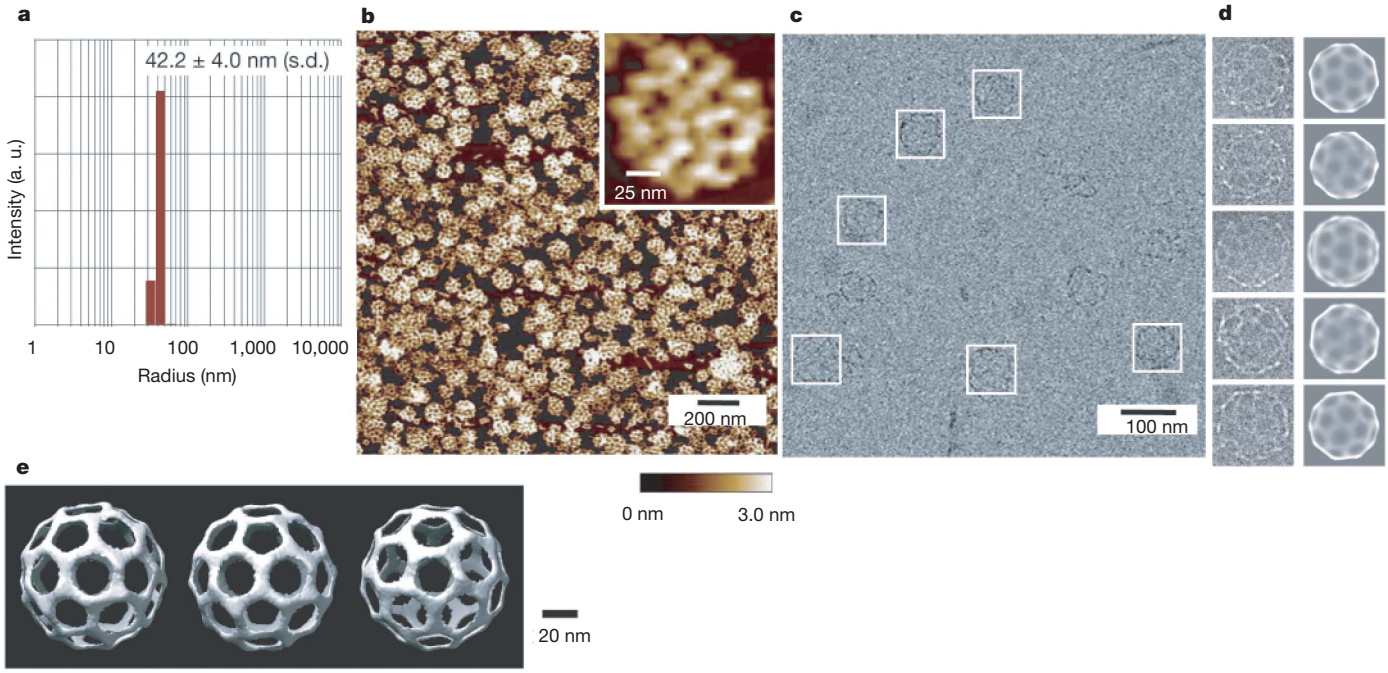

Figure 4 | A DNA buckyball. **a**, Size histogram of the DNA buckyball measured by DLS. **b**, **c**, An AFM image (**b**) and a cryo-EM image (**c**) of the DNA assemblies. For a magnified large view field, see Supplementary Fig. 9. **d**, Individual raw cryo-EM images and the corresponding projections of the DNA buckyball 3D structure reconstructed from cryo-EM images. These particles are selected from different image frames to represent views at different orientations. **e**, Three views of the DNA buckyball structure reconstructed from cryo-EM images.

structural model (41.0 nm). However, the polydispersity of these assemblies is higher than that of the tetrahedron and dodecahedron assemblies. AFM imaging shows the DNA assemblies as uniform-sized, round, collapsed nanostructures with a diameter of ~110 nm. Once again, the most direct evidence for buckyball formation comes from cryo-EM imaging (Fig. 4c and Supplementary Fig. 9). Using hand-picked particles, a buckyball 3D structure can be obtained from reconstruction. However, the size distribution and the distortion of the particles in cryo-EM images look much worse than that from the AFM images. Many smaller particles and some networks are visible. These undesired particles introduce some uncertainties to the reconstruction process and lower the quality of the reconstructed structures. The 3D reconstruction merely represents the average structure of these distorted particles. Nevertheless, the resulting structure resembles a buckyball.

We note that the assembly yield decreases as the size of the target structure increases: the assembly yield for the tetrahedron is ~ 90%, but only 76% for the larger dodecahedron and 69% for the even larger buckyball (as analysed by agarose gel electrophoresis; see Supplementary Figure S2). This trend might be rationalized by the fact that larger structures require more star tiles and are thus more difficult to assemble. However, we also note that in the cryo-EM images of the DNA buckyballs, smaller objects and networks are abundant; this highlights that large structures such as buckyballs are easier to deform and break into open networks or smaller aggregates due to external disturbance (as will occur during sample preparation for imaging). The more demanding assembly and the increased lability are both likely to contribute to the apparently decreasing assembly yield for larger structures. However, the current data are not sufficient to evaluate the specific contribution of each of these factors.

We have shown that DNA can be programmed to assemble into well-defined, regular polyhedra that might find use as synthetic nanocontainers or 3D structural scaffolds. The current study used only DNA three-point-star motifs as primary building blocks, but we are currently investigating whether our hierarchical assembly strategy can be applied to other DNA motifs to prepare an even wider range of 3D objects.

METHODS SUMMARY

Oligonucleotides. DNA sequences were adapted from previous works, which were originally designed by the SEQUIN[19] computer program: central long-strand L (blue-red): aggcaccatcgtaggtttcttgccaggcaccatcgtaggtttcttgccaggcaccatcgtaggtttcttgcc; central long strand L′ (blue-red): aggcaccatcgtaggtttaacttgccaggcaccatcgtaggtttaacttgccaggcaccatcgtaggtttaacttgccaggcaccatcgtaggtttaacttgcc; medium strand M (green): tagcaacctgcctggcaagcctacgatggacacggtaacgcc; short peripheral strand S (black): ttaccgtgtggttgctaggcg.

Formation of DNA complexes. DNA strands were combined according to the correct molecular ratios in a tris-acetic-EDTA-Mg^{2+} (TAE/Mg^{2+}) buffer. Tetrahedron formation used strands L′, M and S; dodecahedron and buckyball formation used strands L, M and S. DNA assembly involved cooling solutions from 95 °C to room temperature over 48 h, using concentrations as indicated in Fig. 1 unless specifically stated otherwise. DNA samples were then directly used for characterization, without further fractionation or purification.

Non-denaturing PAGE and AFM imaging and DLS. Gels containing 4% polyacrylamide were run at 4 °C. For AFM, DNA samples were imaged in tapping-mode on a Multimode AFM with a Nanoscope IIIa controller (Veeco) using oxide-sharpened silicon probes in air at 22 °C. For DLS, 12 μl DNA sample solutions were measured by DynaPro 99 (Protein Solutions/Wyatt) with laser wavelength of 824 nm at 22 °C.

Cryo-EM imaging. DNA sample solutions were concentrated to ~3 μM, spread onto Quantifoil grids, then plunge-frozen. Data were recorded using a Gatan 4,080 × 4,080 pixel charge-coupled device (CCD) camera in a Philips CM200 transmission electron microscope with field-emission gun operating at 200 kV accelerating voltage.

Single-particle reconstruction. 3D reconstructions of the DNA polyhedra used the single-particle image processing software EMAN[18]. Correct symmetry for each of the polyhedra was established by processing the images, assuming different symmetries and finding the symmetry that yields a 3D reconstruction consistent with the particle images (Supplementary Figs 5 and 8). Final 3D maps were visualized using UCSF Chimera software[20].

Full Methods and any associated references are available in the online version of the paper at www.nature.com/nature.

Received 10 July; accepted 18 December 2007.

1. Seeman, N. C. DNA in a material world. *Nature* **421,** 427–431 (2003).
2. Seeman, N. C. DNA enables nanoscale control of the structure of matter. *Q. Rev. Biophys.* **38,** 363–371 (2005).
3. Feldkamp, U. & Niemeyer, C. M. Rational design of DNA nanoarchitectures. *Angew. Chem. Int. Edn Engl.* **45,** 1856–1876 (2006).
4. Adleman, L. M. Molecular computation of solutions to combinatorial problems. *Science* **266,** 1021–1024 (1994).
5. Winfree, E., Liu, F. R., Wenzler, L. A. & Seeman, N. C. Design and self-assembly of two-dimensional DNA crystals. *Nature* **394,** 539–544 (1998).
6. Rothemund, P. W. K., Papadakis, N. & Winfree, E. Algorithmic self-assembly of DNA Sierpinski triangles. *PLoS Biol.* **2,** 2041–2053 (2004).
7. Yan, H., Park, S. H., Finkelstein, G., Reif, J. H. & LaBean, T. H. DNA-templated self-assembly of protein arrays and highly conductive nanowires. *Science* **301,** 1882–1884 (2003).
8. Scheffler, M., Dorenbeck, A., Jordan, S., Wustefeld, M. & von Kiedrowski, G. Self-assembly of trisoligo-nucleotidyls: the case for nano-acetylene and nano-cyclobutadiene. *Angew. Chem. Int. Edn Engl.* **38,** 3312–3315 (1999).
9. Rothemund, P. W. K. Folding DNA to create nanoscale shapes and patterns. *Nature* **440,** 297–302 (2006).
10. Chen, J. H. & Seeman, N. C. Synthesis from DNA of a molecule with the connectivity of a cube. *Nature* **350,** 631–633 (1991).
11. Zhang, Y. W. & Seeman, N. C. Construction of a DNA-truncated octahedron. *J. Am. Chem. Soc.* **116,** 1661–1669 (1994).
12. Shih, W. M., Quispe, J. D. & Joyce, G. F. A 1.7-kilobase single-stranded DNA that folds into a nanoscale octahedron. *Nature* **427,** 618–621 (2004).
13. Goodman, R. P. *et al.* Rapid chiral assembly of rigid DNA building blocks for molecular nanofabrication. *Science* **310,** 1661–1665 (2005).
14. Goodman, R. P., Berry, R. M. & Turberfield, A. J. The single-step synthesis of a DNA tetrahedron. *Chem.* Commun.1372–1373 (2004).
15. Douglas, S. M., Chou, J. J. & Shih, W. M. DNA-nanotube-induced alignment of membrane proteins for NMR structure determination. *Proc. Natl Acad. Sci. USA* **104,** 6644–6648 (2007).
16. He, Y., Chen, Y., Liu, H. P., Ribbe, A. E. & Mao, C. D. Self-assembly of hexagonal DNA two-dimensional (2D) arrays. *J. Am. Chem. Soc.* **127,** 12202–12203 (2005).
17. He, Y. & Mao, C. D. Balancing flexibility and stress in DNA nanostructures. *Chem. Commun.* 968–969 (2006).
18. Ludtke, S. J., Baldwin, P. R. & Chiu, W. EMAN: Semiautomated software for high-resolution single-particle reconstructions. *J. Struct. Biol.* **128,** 82–97 (1999).
19. Seeman, N. C. Denovo design of sequences for nucleic-acid structural engineering. *J. Biomol. Struct. Dyn.* **8,** 573–581 (1990).
20. Goddard, T. D., Huang, C. C. & Ferrin, T. E. Visualizing density maps with UCSF chimera. *J. Struct. Biol.* **157,** 281–287 (2007).

Supplementary Information is linked to the online version of the paper at www.nature.com/nature.

Acknowledgements We thank H. Liu for help with the initial DLS experiment. This work was supported by the National Science Foundation. AFM and DLS studies were carried out in the Purdue Laboratory for Chemical Nanotechnology (PLCN). The cryo-EM images were taken in the Purdue Biological Electron Microscopy Facility and the Purdue Rosen Center for Advanced Computing (RCAC) provided the computational resource for the 3D reconstructions.

Author Information Reprints and permissions information is available at www.nature.com/reprints. Correspondence and requests for materials should be addressed to C.M. (mao@purdue.edu).

METHODS

Oligonucleotides. All oligonucleotides were purchased from IDT, Inc. and purified by 20% denaturing polyacrylamide gel electrophoresis (PAGE).

Formation of DNA complexes. The TAE/Mg^{2+} buffer contained 40 mM Tris base (pH 8.0), 20 mM acetic acid, 2 mM EDTA and 12.5 mM magnesium acetate. At the same DNA concentrations as in Fig. 1, DNA samples were directly used after assembly for AFM imaging and DLS studies, but concentrated to ~3 μM for cryo-EM imaging. No fractionationation or purification was needed after assembly of DNA complexes.

Non-denaturing PAGE. Gels containing 4% polyacrylamide (19:1 acrylamide/bisacrylamide) were run on a FB-VE10-1 electrophoresis unit (FisherBiotech) at 4 °C (100 V, constant voltage). The running buffer was TAE/Mg^{2+} buffer. After electrophoresis, the gels were stained with Stains-All (Sigma) and scanned. PAGE is only suited for characterization of DNA tetrahedra, but not for dodecahedra and buckyballs because these are too large to migrate into the gel matrix.

AFM imaging. A drop of 2 μl DNA solution was spotted onto freshly cleaved mica surface, and kept for 10 s to achieve strong adsorption. The sample drop was then washed off by 30 μl 2 mM magnesium acetate solution, and dried by compressed air. DNA samples were imaged in tapping mode on a Multimode AFM with Nanoscope IIIa controller (Veeco) using oxide-sharpened silicon probes having a resonance frequency in the range of 280–320 kHz (MikroMasch–NSC15). The tip–surface interaction was minimized by optimizing the scan set-point to the highest possible value. AFM imaging was performed at 22 °C.

Cryo-EM imaging. DNA sample solutions were concentrated to ~3 μM (in terms of DNA tiles) with Microcon YM-100 (100 kDa) Centrifugal Filter Units. A drop of 3 μl concentrated DNA solution was pipetted onto a Quantifoil grid. Then, the grid was blotted and immediately plunge-frozen into ethane slush cooled by liquid nitrogen. The images were taken under low-dose condition to minimize radiation damages to the samples. To enhance the image contrast, under-focuses in the range of 2–4 μm were used to record the images. The calibrated magnifications used for DNA tetrahedron, dodecahedron, and buckyballs were ×68,050, ×52,260 and ×37,760, respectively, resulting in pixel sizes of 2.21, 2.87 and 3.97 Å.

Initial model. For all DNA polyhedra, initial models were built using 100 randomly selected raw particles. The initial orientation of individual particle was randomly assigned within the corresponding asymmetry unit of the polyhedron.

DNA tetrahedron. 449 particles were used for the single-particle reconstruction. 110 reference projections in the tetrahedral asymmetric unit were generated at an angular interval of 4°. A projection matching algorithm was then used to determine the centre and orientation of raw particles in the iterative refinement. The tetrahedral symmetry was imposed during the reconstruction. The map resolution was determined to be at 2.6 nm using the Fourier shell correlation (0.5 threshold criterion) of two 3D maps independently built from half data sets. Control reconstructions without imposing any symmetry or with lower symmetries imposed were performed to check that particles indeed have tetrahedron symmetry (Supplementary Fig. 3).

DNA dodecahedron. 725 particles were used for the single-particle reconstruction. 99 reference projections were generated in the icosahedral asymmetric unit with an angular interval of 2°. A projection matching algorithm was used to determine the particle centre and orientation. Icosahedral symmetry was imposed during reconstruction. The final resolution and map quality were evaluated as those of the DNA tetrahedron, indicating a resolution of 2.8 nm.

DNA buckyball. 514 particles were used for the buckyball reconstruction. 30 reference projections resulted from an angular interval of 4° in an icosahedral asymmetric unit. Icosahedral symmetry was imposed during reconstruction.